

Chapter 6 - Relaxation Phenomena in the ZrTiBe System

6.1 Abstract

The presence of two apparent glass transitions in the large ΔT alloys prompted further investigation of flow and relaxation properties in the supercooled liquid region (SCLR). This chapter is similar to a paper entitled “Relaxation Phenomena in the ZrTiBe System” submitted to Acta Materialia. The expected authors are [A. Wiest, S. Roberts, M.L. Lind, D. Soh, D.C. Hofmann, M.D. Demetriou, C.M. Garland, W.L. Johnson]. The discovery of bulk glass forming compositions in the ZrTiBe system allowed a more thorough study of relaxation phenomena in the SCLR to be accomplished. Heat capacity measurements of glassy compositions show two discontinuities, Δc_{p1} and Δc_{p2} , in the SCLR. If the discontinuities are assumed to arise from glass transitions of two glasses with similar fragilities and different glass transition temperatures then the ratio $\Delta c_{p1}/(\Delta c_{p1} + \Delta c_{p2})$ gives the fraction of the first glassy phase. A plot of $\Delta c_{p1}/(\Delta c_{p1} + \Delta c_{p2})$ vs Zr concentration along an iso Be line reveals a linear relationship and rule of mixtures analysis predicts compositions that would be single phase. The predicted compositions exhibit single phase glass behavior and glass transition temperatures consistent with the two phase alloys. Viscosity vs temperature and shear modulus versus temperature measurements also reveal relaxation events at temperatures near the observed jumps in heat capacity. These relaxation events are well described by a two phase glass assumption, but microstructural evidence is lacking.

6.2 Introduction

The existence of a miscibility gap in the SCLR of BMG that gives rise to phase separation upon relaxation of the glass has been claimed in many glass forming alloy

systems including AuPbSb [1-2], ZrCu [3], ZrTiBe [4-7], ZrTiCuNiBe [8-10], MgCuYLi [11], CuZrAlAg [12], TiYAlCo and ZrYAlCo [13]. Using X-ray scattering, Johnson and collaborators detected splitting of the broad amorphous spectrum in an as-spun AuPbSb glassy ribbon [1]. Additional studies using Small Angle Neutron Scattering (SANS) [9-10], Small Angle X-ray Scattering (SAXS) [10], Anomalous Small Angle X-ray Scattering (ASAXS) [11], Transmission Electron Microscopy (TEM) [13], discontinuous slopes in resistivity measurements [3], and Differential Scanning Calorimetry (DSC) [4-7] have been performed to support the apparent phase separation in many glass forming systems. In some systems, such as in the Vitreloy (ZrTiNiCuBe) system, phase separation arises by annealing the glassy phase below T_g , supporting the existence of a miscibility gap below T_g [8-10]. In other systems, such as AuPbSb and ZrTiBe, phase separation is manifested as a twin relaxation in the SCLR [1-2, 4-7], supporting the idea that the miscibility gap extends above T_g , and suggesting that perhaps two chemically separable glassy phases vitrify upon cooling the alloy below the miscibility gap.

Tanner examined the ZrTiBe system for glass forming compositions and found that many alloys could form amorphous ribbons with thickness up to $100\mu\text{m}$ [14-15]. Heat capacity measurements using DSC revealed that some of the glassy alloys exhibit two discontinuities in heat capacity upon heating. Typically, a glassy material upon heating is expected to exhibit just one discontinuity in heat capacity that designates the increase in mobility associated with the glass relaxing to a supercooled liquid state at T_g [16]. A double jump in heat capacity, which can be interpreted as a double glass transition temperature is unusual. Tanner proposed that this anomalous feature of the heat capacity supports the coexistence of two glassy phases in the vitrified state. Other

authors who have studied this system have interpreted the second jump in specific heat as an exothermic ordering event that follows T_g and precedes crystallization [17]. To date, the precise origin of the double jump in heat capacity and the associated impact on the chemistry, structure, and rheology of the supercooled liquid remain unresolved, a fact that can be at least partly attributed to the unavailability of bulk ZrTiBe specimens.

Recently, the ZrTiBe system has been reexamined, and many compositions that exhibit the apparent two T_g phenomenon and which were previously thought to be limited to a critical casting thickness of 100 μ m could in fact be cast into bulk glassy samples with thicknesses that range from 1 - 6mm [18]. The availability of bulk ZrTiBe samples that exhibit two T_g events paves the way to a more thorough examination of this phenomenon allowing measurement of bulk flow properties and shear modulus as a function of temperature. We use bulk ZrTiBe specimens to investigate the effects of the two T_g events on the heat capacity, rheology, and rigidity of the SCLR through DSC, TMA, and ultrasonic tests.

6.3 Experimental Method

Elements of 99.9% purity or higher were arc melted on a water cooled copper hearth under a Ti-gettered argon atmosphere. Zr and Ti were varied in 5 atomic percent increments along a fixed Be line and compositions were cast into 0.5mm thick plates for DSC analysis using an Edmund Buhler mini arc melter. The amorphous nature of the plates was verified using X-ray diffraction. Segments from the plates were heated in a Netzsch 404C Pegasus Differential Scanning Calorimeter at 20 K/min and 5 K/min past the crystallization temperature. The 20 K/min scans showed sharper features in heat capacity because of the larger signal produced at faster scan rates and 20 K/min scans

were used to determine the apparent glass transition temperatures and magnitude of the jumps in heat capacity. To enable the evaluation of the heat capacity jump from the 20 K/min scans, an initial baseline was taken and then subtracted from the sample run. The 5 K/min runs were used to determine the glass transition temperatures at that rate, as the viscosity and shear modulus experiments were conducted at 5 K/min. Since only T_g was of interest at 5 K/min, baseline subtraction was unnecessary.

The heat capacity features of the SCLR were analyzed in a consistent manner. A baseline heat capacity is seen at low temperatures, and two successive jumps in heat capacity are seen before the exothermic crystallization event. The lower glass transition temperature, T_{g1} is defined as the intersection between the tangent to the low temperature heat capacity baseline and the tangent to the point of steepest slope during the first heat capacity jump. The second heat capacity jump is similarly analyzed to find the second glass transition temperature, T_{g2} . The two jumps in heat capacity are denoted Δc_{p1} and Δc_{p2} , and are shown in Figure 6.1.

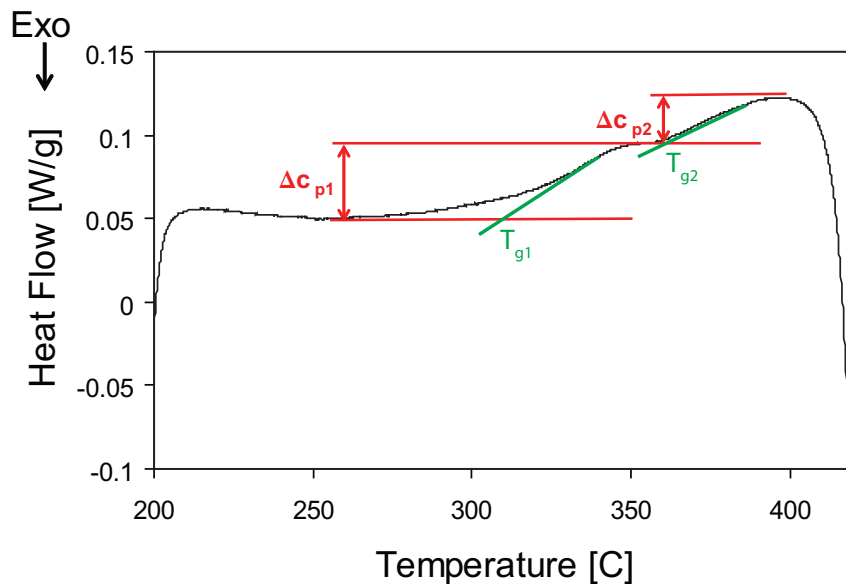


Figure 6.1: 20 K/min DSC scan of $Zr_{30}Ti_{30}Be_{40}$ showing double discontinuity in heat capacity in SCLR. Δc_p and T_g determination method illustrated.

The viscosity was measured using the parallel plate geometry with a Perkin Elmer Diamond TMA over a temperature region spanning the two T_g events. 1mm and 3mm diameter specimens were used. The diameter to height aspect ratio was set to 1.0 for the 3mm diameter samples, and to 1.8 for the 1mm diameter samples to avoid buckling and achieve maximum deformation. A force of 1400 mN was applied resulting in a compressive stress of 1.8 MPa on the 1mm diameter specimens and a stress of 0.2 MPa on the 3mm diameter specimens. The heating rate through the SCLR was 5 K/min. The viscosity was analyzed using the displacement and the displacement time derivative data, according to the method for parallel plate rheometry also known as Stefan's equation found in Derivation 3 and [19]. The condition of zero thickness was not approximated in this study, as suggested in [19] for accurate viscosity determination. Nevertheless, despite a limited accuracy in viscosity, the relative flow behavior of different alloys, which is of interest here, is clearly revealed by the present data.

In situ pulse-echo ultrasonic measurements using 25 MHz shear transducers (Ultran) were used to measure the shear sound velocity of 8mm diameter rods heated from room temperature through 410 °C with a heating rate of approximately 5 K/min. The detailed experimental setup is fully described in Lind's Caltech PhD Dissertation [20].

Samples were prepared for TEM by dimple grinding 50 μ m thick foils from both sides and then ion milling. The ion milling was done at -100 °C, 9 degrees milling angle, 3.5kV and 7.0mA. Diffraction patterns were obtained as well as bright field and dark field images at 1400000x.

6.4 Results and Discussion

6.4.1 Heat Capacity Measurements

A DSC scan conducted at 20 K/min of a $Zr_{30}Ti_{30}Be_{40}$ alloy is presented in Figure 6.1. If we assume two phases, then the ratio $\Delta c_{p1}/(\Delta c_{p1} + \Delta c_{p2})$ should give some information about the fraction of phase one in the alloy. To determine what information can be gained, a brief discussion of fragility is necessary.

Fragility (m) is a measure of a liquid's resistance to flow with temperature, or put differently, a resistance to changes in medium range order. Mathematically,

$m = \frac{\partial \text{Log}(\eta)}{\partial (T_g/T)}$ which is the slope of the $\text{Log}(\eta(T_g/T))$ curve. A liquid with low fragility

resists flow and therefore has a lower configurational entropy (S_{config}) than a more fragile liquid [16]. Liquids with low fragilities exhibit smaller jumps in heat capacity at the glass transition temperature because $T^* \Delta c_p = S_{\text{config}}$. Therefore, the fraction of phase one is given by the ratio $\Delta c_{p1}/(\Delta c_{p1} + \Delta c_{p2})$ if the two liquids are assumed to have similar fragilities.

More thorough examination of the ZrTiBe system reveals many compositions with moderate GFA = 1 - 6mm that exhibit apparent double glass transitions, similar to the $Zr_{36}Ti_{24}Be_{40}$ alloy, upon heating in the DSC. The alloys with the best GFA are along the $(Zr_aTi_{1-a})_{65}Be_{35}$ composition line, but larger variations in fraction of phase 1 as a function of composition are found along the $(Zr_aTi_{1-a})_{60}Be_{40}$ line. The data is analyzed using the similar fragility assumption so that the fraction of phase 1 = $\Delta c_{p1}/(\Delta c_{p1} + \Delta c_{p2})$. A plot of $\Delta c_{p1}/(\Delta c_{p1} + \Delta c_{p2})$ versus Zr concentration is found in Figure 6.2 for the Be = 35 and Be = 40 pseudo binary lines. Linear fits are included in Figure 6.2 and have R^2 values greater than 0.99. The goodness of fit of the linear relationship suggests that a rule

of mixtures analysis could be applied to determine the compositions where a single phase alloy would be expected. The compositions into which the alloy appears to be phase separating are given by $\Delta c_{p1}/(\Delta c_{p1} + \Delta c_{p2}) = 1$ for all phase 1 and $\Delta c_{p1}/(\Delta c_{p1} + \Delta c_{p2}) = 0$ for all phase 2.

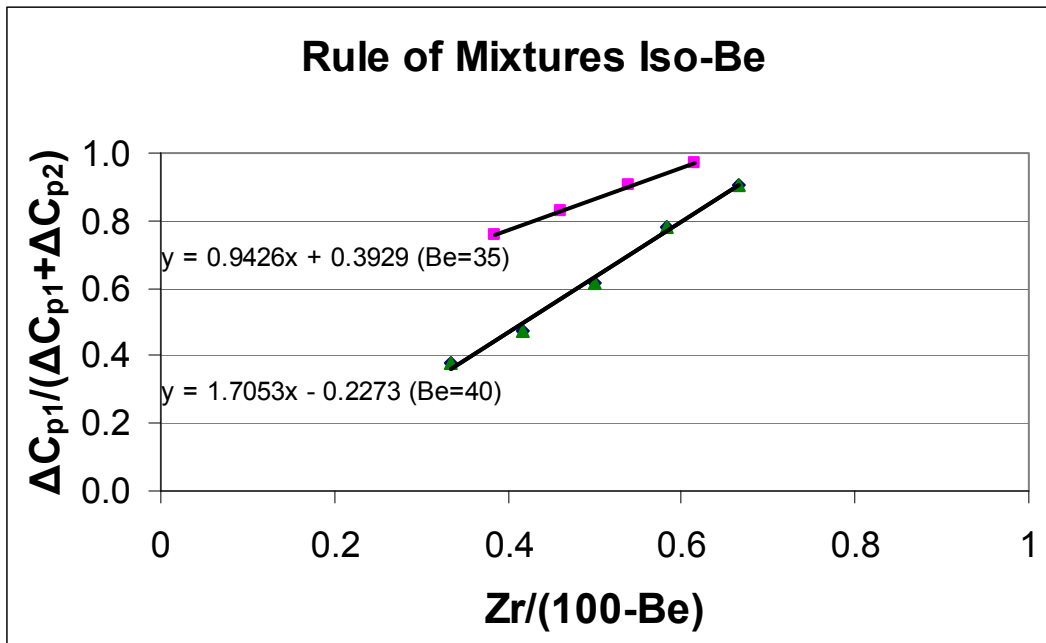


Figure 6.2: Plot of $\Delta c_{p1}/(\Delta c_{p1} + \Delta c_{p2})$ versus Zr concentration gives fraction of phase 1 assuming two glassy phases with similar fragilities. Linear fits indicate rule of mixtures analysis is appropriate and suggests a metastable miscibility gap in SCLR.

Along the Be = 35 line we extrapolate to the point where $\Delta c_{p1}/(\Delta c_{p1} + \Delta c_{p2}) = 1$ and find that the composition $Zr_{42}Ti_{23}Be_{35}$ should exhibit a single jump in heat capacity at T_{g1} but unfortunately, the variation in $\Delta c_{p1}/(\Delta c_{p1} + \Delta c_{p2})$ versus Zr concentration is not steep enough to find a composition where $\Delta c_{p1}/(\Delta c_{p1} + \Delta c_{p2}) = 0$. In Table 6.1, we see that near the composition predicted to show all phase 1 along the Be = 35 line, alloys do not have a visible second jump in heat capacity. However, along the Be = 40 line we can extrapolate to compositions where $\Delta c_{p1}/(\Delta c_{p1} + \Delta c_{p2})$ equals 1 or 0. These compositions are $Zr_{43}Ti_{17}Be_{40}$ for all phase 1 and $Zr_8Ti_{52}Be_{40}$ for all phase 2. The GFA of the

Zr₈Ti₅₂Be₄₀ alloy was poor and an amorphous sample was obtainable only in thin foils. The DSC scans of Zr₄₅Ti₁₅Be₄₀ and Zr₈Ti₅₂Be₄₀ and a two phase glass midway along the composition line Zr₃₀Ti₃₀Be₄₀ are shown in Figure 6.3. The rule of mixtures analysis predicted the compositions where a single phase glass would exist and we now have some evidence of the compositions that the two phase glasses are separating into. Note that the glass transition temperatures of each phase are fairly consistent between the two phase and single phase glasses and that the overall jumps in heat capacity $\Delta c_{p1} + \Delta c_{p2}$ are similar along each iso Be line. The Zr₈Ti₅₂Be₄₀ alloy likely exhibits a smaller $\Delta c_{p1} + \Delta c_{p2}$ value because of early onset of crystallization. Thermodynamic data of the compositions including glass transition temperatures and Δc_p values is found in Table 6.1.

Table 6.1: DSC data for alloys considered in this article. Data shown in parentheses taken at 5 K/min. Other data taken at 20 K/min. Temperatures in °C. Δc_{p1} values in J/(g*K).

Composition	T _{g1}	Δc_{p1}	T _{g2}	Δc_{p2}	$\Delta c_{p1}/(\Delta c_{p1} + \Delta c_{p2})$
Zr ₂₅ Ti ₄₀ Be ₃₅	301.7	0.275	362	0.089	0.76
Zr ₃₀ Ti ₃₅ Be ₃₅	304.1	0.328	364.1	0.069	0.83
Zr ₃₅ Ti ₃₀ Be ₃₅	305.7	0.366	364.4	0.039	0.90
Zr ₄₀ Ti ₂₅ Be ₃₅	303.7	0.339	367.3	0.01	0.97
Zr ₄₅ Ti ₂₀ Be ₃₅	303.2	0.43	N/A	0	1
Zr ₈ Ti ₅₂ Be ₄₀	N/A	0	379.9	0.25	0
Zr ₂₀ Ti ₄₀ Be ₄₀	324.9 (320)	0.167	377.6 (363)	0.271	0.38
Zr ₂₅ Ti ₃₅ Be ₄₀	319.0 (311)	0.198	379.3 (360)	0.218	0.48
Zr ₃₀ Ti ₃₀ Be ₄₀	323.6 (317)	0.261	375.2 (360)	0.164	0.61
Zr ₃₅ Ti ₂₅ Be ₄₀	312.2	0.303	377.8	0.086	0.78
Zr ₄₀ Ti ₂₀ Be ₄₀	319.3	0.346	374.5	0.035	0.91
Zr ₄₅ Ti ₁₅ Be ₄₀	323.9	0.344	N/A	0	1
Zr ₃₀ Ti ₃₀ Be ₃₂ Cu ₈	(306)		(355)		

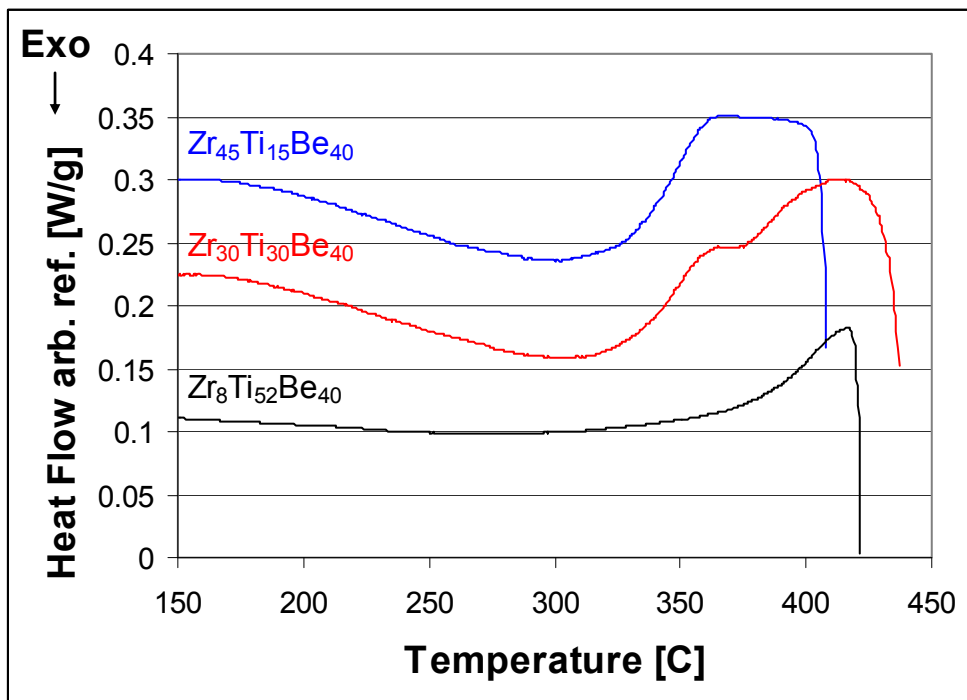


Figure 6.3: 20 K/min DSC scans of alloys predicted to show only one phase from rule of mixtures analysis and one intermediate two phase composition.

It is interesting to note that both the simple ZrTiBe glasses and the quinary Vitreloy compositions appear to separate into a Zr rich and a Ti rich phase. The ZrTiBe glasses differ from the Vitreloy glasses in that they exhibit the two phase behavior without any annealing in the SCLR. This suggests that the phase separation is more favorable in the ternary system. It is also likely that annealing causes the glass to relax toward the stable crystal phase as was seen in the Vitreloy glasses. This data lends itself to expression in a metastable phase diagram exhibiting a liquid miscibility gap with the endpoint compositions $Zr_8Ti_{52}Be_{40}$ and $Zr_{43}Ti_{17}Be_{40}$. The metastable phase diagram is shown in Figure 6.4.

Miscibility Gap $\text{Be} = 40$

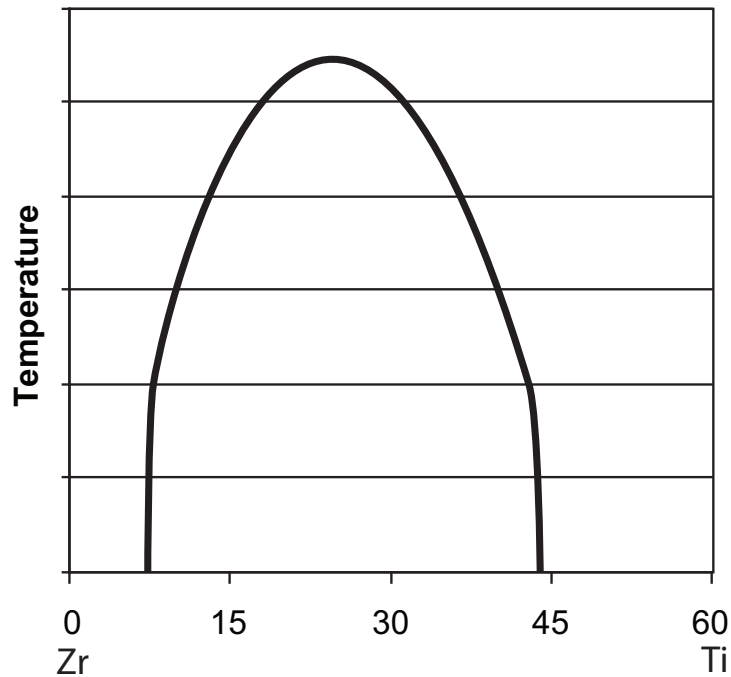


Figure 6.4: Sketch of the metastable miscibility gap in SCLR of $(\text{Zr}_a\text{Ti}_{1-a})_{60}\text{Be}_{40}$. Endpoint compositions are known, but temperature bounds are not.

The explanation of the apparent double T_g as a single T_g with an exothermic ordering event would be more plausible if only the glass exhibiting all phase 1 at $\text{Zr}_{43}\text{Ti}_{17}\text{Be}_{40}$ had been found. In this case, one could argue that the ordering event becomes less and less thermodynamically favorable as Zr content increases until the transition disappears. However, given the discovery of the $\text{Zr}_8\text{Ti}_{52}\text{Be}_{40}$ composition that shows only one jump in heat capacity at the temperature corresponding to the apparent T_{g2} , this exothermic ordering event explanation seems unlikely. While the present work does not prove the existence of two glassy phases in this system, it does present convincing evidence that a two phase glass is the most likely explanation. In the rest of this article, the assumption of a two phase glass is made to explain the observed phenomena.

6.4.2 Rheology

The flow of liquids with multiple phases is most simply divided into two limiting cases for ideal mixtures. Variations of these ideal cases have been proposed to explain the flow of other types of liquid mixtures. Very complicated analysis is possible for non-Newtonian effects and can consider interfacial energies between the layers, but we seek a qualitative picture of what to expect from viscosity as a function of temperature plots. Both cases consider a liquid mixture with parallel layers or laminae. The applied shear stress is orthogonal to the layers in Case 1. The applied shear stress is parallel to the layers in Case 2. A simple analysis of these cases can be found in Derivation 8 and [21]. The results of the analysis find that viscosities, η , are additive for fluid mixtures resembling Case 1, and fluidities, $\phi = 1/\eta$, are additive for mixtures resembling Case 2. The measured viscosity is just a volume weighted average of the individual component viscosities or fluidities depending on which case better approximates the mixture of interest. This resembles the analysis of resistors in series or parallel. In immiscible fluids, the layers resist indefinite extension and a case similar to Case 1 results [21].

In the two phase amorphous $(Zr_aTi_{1-a})_{60}Be_{40}$ alloys, one would expect to see three regions of flow. The first region is at temperatures below T_{g1} where the sample would behave like a solid and little or no flow would be observed. The second region covers the temperature range $T_{g1} < T < T_{g2}$. In region 2, we should see a slope change in the viscosity versus temperature curve as the liquid + solid solution begins flow. The third region spans the temperature range $T_{g2} < T < T_x$. In region three, the sample should exhibit flow characteristic of a two phase liquid. The sample begins to crystallize and flow stops at T_x . Therefore, a flat $\eta(T)$ relationship is expected in region one, followed

by a slightly decreasing $\eta(T)$ slope in the solid + liquid solution in region 2, and finally a large decrease in the $\eta(T)$ slope in region 3 as both liquids begin to soften and flow. Additionally, we should see a compositional effect causing lower measured values of viscosity for a given temperature in alloys with a larger fraction of the low T_g phase. The three regions should be visible in the $\eta(T)$ plots regardless of whether the alloys exhibit flow characteristics governed by additive viscosity or additive fluidity cases.

Three alloys along the $\text{Be} = 40$ line with moderate GFA and varying fractions of the two phases were chosen to examine the flow characteristics of the alloys in the two phase region. The chosen alloys were $\text{Zr}_{20}\text{Ti}_{40}\text{Be}_{40}$, $\text{Zr}_{25}\text{Ti}_{35}\text{Be}_{40}$, and $\text{Zr}_{30}\text{Ti}_{30}\text{Be}_{40}$ with 35%, 48%, 61% of phase 1 respectively (as measured by the $\Delta c_{p1}/(\Delta c_{p1} + \Delta c_{p2})$ method). Plots of $\eta(T)$ are shown for the three alloys in Figure 6.5. The three flow regions are visible in the plots and correlate well to the T_g values measured at the same heating rate in the DSC. We also see the composition effect causing lower measured viscosities at a given temperature for alloys with higher fractions of the low T_g phase. The horizontal region in the $\eta(T)$ plots at T_{g2} is not understood and may be due to the small diameter of the samples tested.

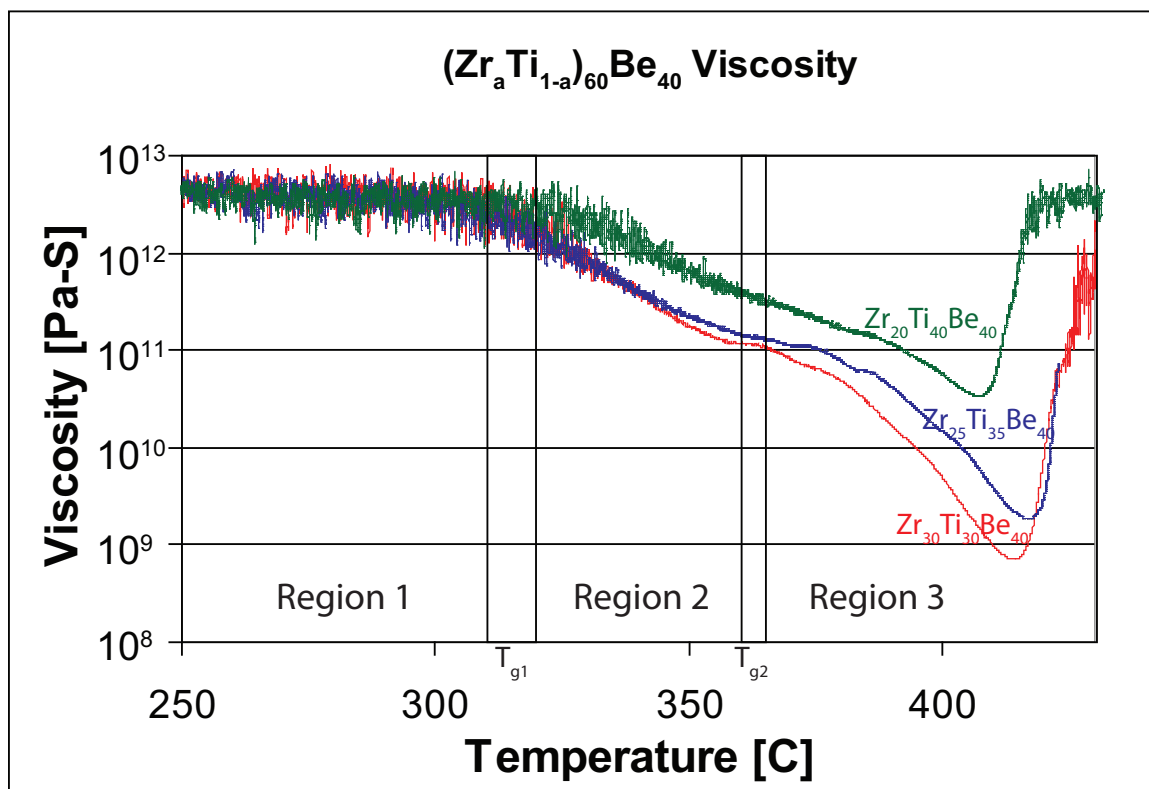


Figure 6.5: $\eta(T)$ plots for three alloys with differing fractions of phase 1, showing apparent double glass transition. The test specimens were 1mm diameter x 1.8mm tall rods of $Zr_{20}Ti_{40}Be_{40}$ (38% phase 1), $Zr_{25}Ti_{35}Be_{40}$ (48% phase 1), and $Zr_{30}Ti_{30}Be_{40}$ (61% phase 1) deformed under a force of 1400 mN at 5 K/min in a TMA. Region 1 corresponds to a solid-solid mixture with no deformation. Region 2 corresponds to solid-liquid mixture and minimal deformation indicated by shallow slope of $\eta(T)$. Region 3 is a liquid-liquid mixture with the greatest deformation rate indicated by the steepest $\eta(T)$ slope. The scatter in first and second glass transitions as measured in 5 K/min DSC scans shown by parallel black vertical lines.

Additions of Cu were found to increase the GFA and the temperature range of the SCLR while maintaining the two discontinuities in heat capacity for some of these alloys. 3mm diameter samples of $Zr_{30}Ti_{30}Be_{32}Cu_8$ were cast fully amorphous and $\eta(T)$ was measured for as-cast samples and samples annealed at 410 °C for 100 s above T_{g2} . $Zr_{30}Ti_{30}Be_{32}Cu_8$ has 63% phase 1 as measured by the $\Delta c_{p1}/(\Delta c_{p1} + \Delta c_{p2})$ method. $\eta(T)$ plots for the as-cast and annealed samples are shown in Figure 6.6. The $\eta(T)$ plots are very similar for both samples. Three flow regions are again visible and the horizontal region after T_{g2} is not present. The transition from the first to the second flow region

happens at T_{g1} as expected, but the second decrease in slope of $\eta(T)$ does not happen until 50 degrees above T_{g2} .

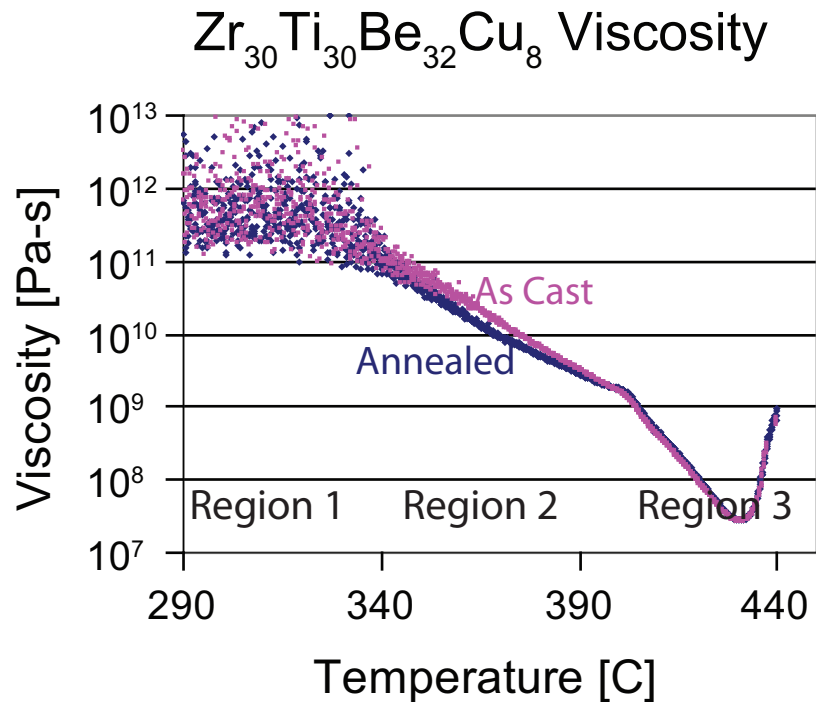


Figure 6.6: $\eta(T)$ plots for as-cast and annealed samples of $Zr_{30}Ti_{30}Be_{32}Cu_8$. The test specimens were 3mm diameter x 3mm tall rods deformed under a force of 1400 mN at 5 K/min in a TMA. The annealed sample was heated to 410 °C for 100 s and shows a slightly lower viscosity than the as-cast sample in region 2. Both samples show similar flow behavior in the SCLR. The flow regions and glass transitions do not align for these samples as was observed for the $(Zr_aTi_{1-a})_{60}Be_{40}$ compositions in Figure 6.5.

Viscosity versus temperature measurements show two relaxation events as would be expected by a two phase glass. These relaxation events are evidenced by changes in the slope of the viscosity vs temperature curves but the slope change does not happen at T_{g2} as one would expect.

6.4.3 Shear Modulus

The shear modulus as a function of temperature $G(T)$ provides another method to observe relaxation phenomena in the SCLR of glasses. As a glass transitions from solid-like to liquid-like behavior at the glass transition temperature, a softening in shear

modulus occurs [16]. In a two phase glass, one would expect two softening events corresponding to the two glass transition temperatures. Two in situ shear modulus measurements were conducted on the $Zr_{30}Ti_{30}Be_{32}Cu_8$ alloy. The first measurement was masked by deformation of the glass in the SCLR because the samples height decreased as it expanded to tightly fill the holder. The second measurement gave $G(T)$ for a sample heated past T_{g2} once. The second $G(T)$ measurement is shown in Figure 6.7. There are two changes in the slope of $G(T)$ roughly corresponding to the two glass transition temperatures. This is another evidence of two relaxation events in the SCLR of these alloys showing the apparent double glass transition.

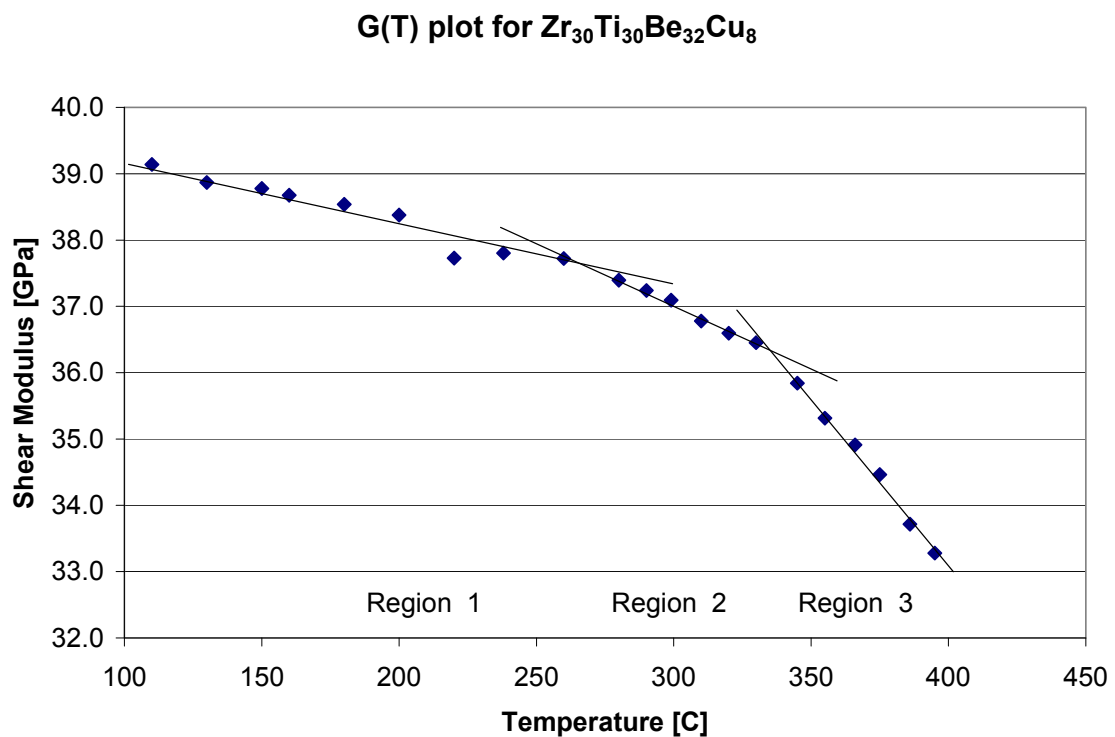


Figure 6.7: In situ $G(T)$ measurements on an annealed sample of $Zr_{30}Ti_{30}Be_{32}Cu_8$ showing two slope changes. These slope changes are indicative of two relaxation events in the alloy. The $G(T)$ and $\eta(T)$ relaxation temperatures do not correlate well for this sample.

It should be noted that the $G(T)$ and $\eta(T)$ relaxation temperatures do not correlate well with each other or with the temperatures corresponding to the heat capacity discontinuities observed in 5 K/min DSC scans. This could be an effect of differences in casting thickness between the samples. DSC and TMA samples were 3mm diameter rods and the sample cast for $G(T)$ measurements was an 8mm rod. The relaxation events however were consistent in $\eta(T)$ measurements for as-cast and annealed samples. Further investigation is warranted to determine the reason behind the large scatter in measured relaxation temperatures.

6.4.4 Microscopy

One would expect good Z contrast in alloys separating into the Zr rich and Ti rich phases proposed in this paper. No Z contrast was visible with SEM imaging using a back scatter electron detector suggesting that phase separation may be smaller than the resolution of the SEM (about 100nm using our polishing technique). This would be consistent with the 13nm length scale phase separation found in the SANS work of Johnson [10]. A representative bright field image, dark field image, and diffraction pattern is included in Figure 6.8 for TEM observation of an ion milled $Zr_{30}Ti_{30}Be_{40}$ specimen. The magnification on the TEM images is 1400000x. Z contrast imaging was attempted using a high angle annular dark field detector, but the lack of contrast made focusing and magnification difficult so no images were obtained. It is not clear that any broadening of the amorphous halos is present in the diffraction pattern. Elemental analysis using electron dispersive X-ray spectroscopy (EDS) in the TEM was unable to detect Be because of experimental limitations, but found that Zr concentration varied from 52 - 58 atomic percent with Ti making the balance. The alloy we imaged was

$Zr_{30}Ti_{30}Be_{40}$ so one would expect $Zr = 50\%$ in a single phase sample, but this deviation from 50% is not statistically significant.

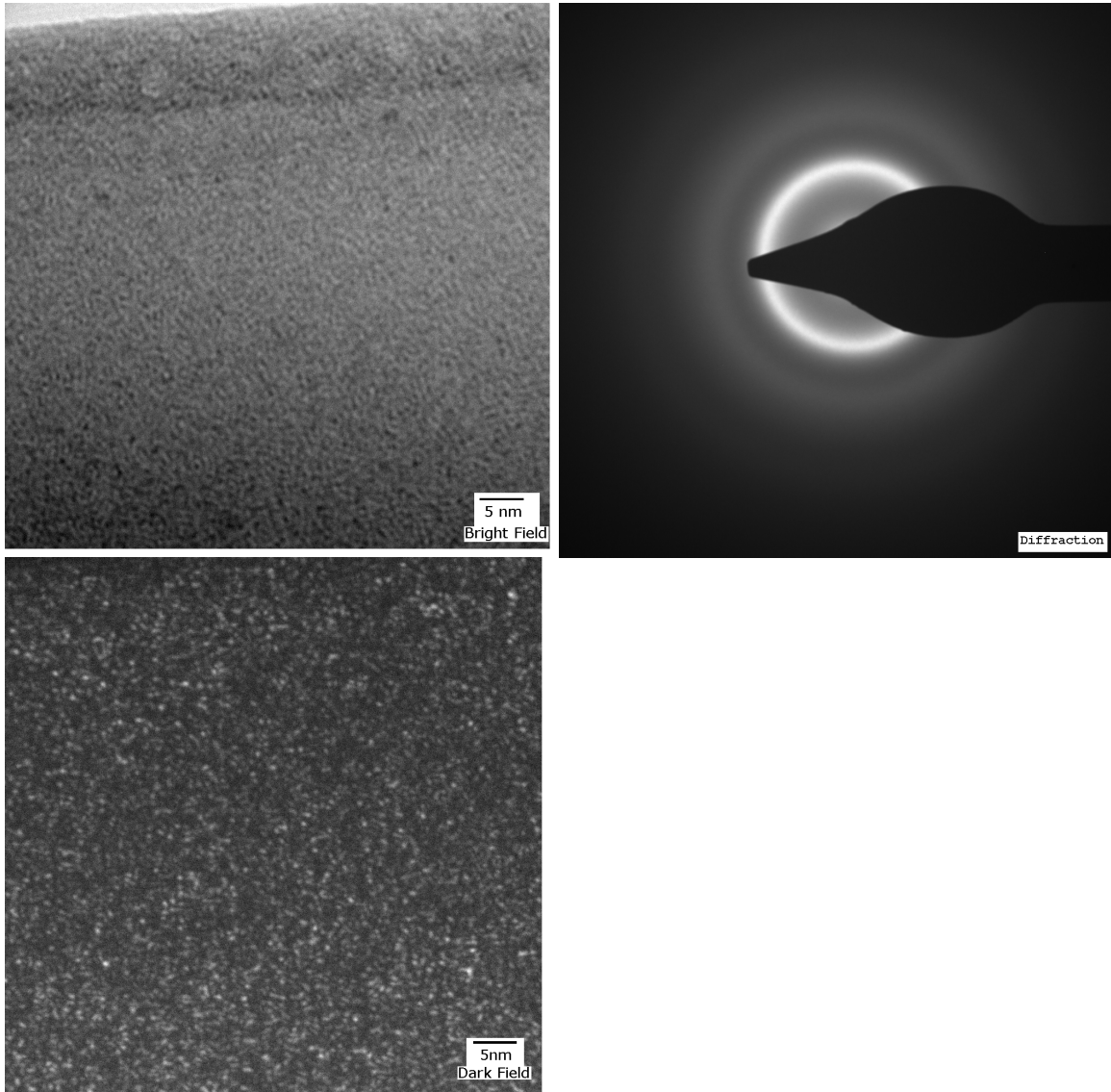


Figure 6.8: Dimple ground and ion milled sample imaged in TEM. Bright field and dark field images show no evidence of two phases. The diffraction pattern is characteristic of an amorphous alloy.

The lack of microscopic evidence does not preclude the existence of two phases, but it casts doubt on the likelihood that two phases are present. It is possible that ion

milling provides enough energy to randomize the two phase structure. Indeed, higher voltages and currents along with longer milling times caused another sample to nanocrystallize in regions. A well prepared, thin TEM sample is about 50nm thick. The length scale of phase separation is bounded below by the size of an STZ. If we assume a 5nm length scale, about half that observed in Vitreloy alloys, we could expect a TEM image averaged over ~ 10 phase separated regions.

6.5 Conclusion

The discovery that many alloys in the ZrTiBe system could be cast amorphous in bulk samples allowed relaxation phenomena in the SCLR to be studied more thoroughly. Heat capacity measurements in a DSC were conducted on many compositions along the Be = 35 and Be = 40 pseudo binary lines. An anomalous double discontinuity in heat capacity in the SCLR was observed. The heat capacity discontinuities were assumed to arise from two glassy phases with different glass transition temperatures and similar fragilities. Under these assumptions, the ratio $\Delta c_{p1}/(\Delta c_{p1} + \Delta c_{p2})$ gives the fraction of phase 1 in the glass. A plot of $\Delta c_{p1}/(\Delta c_{p1} + \Delta c_{p2})$ versus composition reveals a linear relationship suggesting a rule of mixtures analysis would be appropriate and revealing a metastable miscibility gap in the SCLR. Extrapolating the line to $\Delta c_{p1}/(\Delta c_{p1} + \Delta c_{p2}) = 1$ gives the composition $Zr_{43}Ti_{17}Be_{40}$ where we would expect all phase 1. Extrapolating the line to $\Delta c_{p1}/(\Delta c_{p1} + \Delta c_{p2}) = 0$ gives the composition $Zr_8Ti_{52}Be_{40}$ where we would expect all phase 2. DSC scans of amorphous samples of the projected single phase compositions showed a single discontinuity in heat capacity with glass transition temperatures similar to those observed in the intermediate composition range “two phase” alloys.

Viscosity measurements as a function of temperature also revealed two relaxation phenomena. $\eta(T)$ plots showing regions corresponding to solid-solid solutions, solid-liquid solutions, and liquid-liquid solutions were found for three $(\text{Zr}_a\text{Ti}_{1-a})_{60}\text{Be}_{40}$ compositions exhibiting the apparent two glass transitions. The $\eta(T)$ plots also showed lower viscosities as a function of temperature for alloys with a higher concentration of the low T_g , Zr rich, phase. The temperatures at which the flow behavior changed roughly correlate to the apparent glass transition temperatures measured in the DSC. A quaternary composition exhibiting the apparent two glass transitions also showed the three regions of flow. Annealing above the second glass transition temperature did not affect the flow behavior of the quaternary glass.

In situ measurements of shear modulus as a function of temperature, $G(T)$, on the quaternary glass also revealed two relaxation phenomena. Decreases in the slope of the $G(T)$ line indicated softening events and roughly correlated to measured glass transition temperatures in the DSC.

Unfortunately, attempts to image the phases in SEM and TEM were unsuccessful. If the sample thickness was larger than the length scale of phase separation, the resolution of the phases would be diminished in BF and DF imaging as electron interactions are averaged over multiple phase regions. Future work should look for evidence of composition fluctuations using small angle scattering techniques.

The low GFA of the ZrTiBe compositions makes preparation of sufficient sample for SANS difficult. SAXS and ASAXS may provide a suitable alternative method to determine the length scale of any possible phase separation. Evidence of two relaxation events in the SCLR is clear from the presented data. It is still unproven whether or not

the relaxation events arise from two glassy phases softening at T_g . It is unlikely that an explanation proposing a single glass transition with an exothermic ordering event would be sufficient to describe the relaxation phenomena observed in these experiments.

The observed double relaxation phenomena in the SCLR of the studied alloys are not yet fully understood. A two phase glass is one plausible explanation, but more microstructural evidence is needed to confirm this hypothesis.

Chapter 6 References

- [1] M.C. Lee, J.M. Kendall, W.L. Johnson, *Appl. Phys. Lett.* 40 (1982) 382.
- [2] W.L. Johnson, *Amorphe Metallische Werkstoffe 14. Metalltagung in der DDR* (1981) 183.
- [3] R. Schulz, K. Samwer, W.L. Johnson, *J. Non-Cryst. Solids* 61 & 62 (1984) 997.
- [4] L.E. Tanner, R. Ray, *Scripta Metall.* 11 (1977) 783.
- [5] R. Hasegawa, L.E. Tanner, *Phys. Rev. B* 16 (1977) 3925.
- [6] L.E. Tanner, R. Ray, *Acta Metall.* 27 (1979) 1727.
- [7] L.E. Tanner, R. Ray, *Scripta Metall.* 14 (1980) 657.
- [8] S. Schneider, P. Thiyagarajan, U. Geyer, W.L. Johnson, *MRS Technical Report DOI 10.2172/510428* (1996).
- [9] S. Schneider, P. Thiyagarajan, U. Geyer, W.L. Johnson, *Physica B* 241 (1998) 918.
- [10] S. Schneider, U. Geyer, P. Thiyagarajan, W.L. Johnson, *Materials Science Forum Vols. 235-238* (1997) 337.
- [11] W. Liu, W.L. Johnson, S. Schneider, U. Geyer, P. Thiyagarajan, *Phys. Rev. B* 59 (1999) 11755.
- [12] Q. Zhang, W. Zhang, G. Xie, A. Inoue, *Mater. Sci. Eng. B* 148 (2008) 97.
- [13] B.J. Park, H.J. Chang, D.H. Kim, W.T. Kim, K. Chattopadhyay, T.A. Abinandanan, S. Bhattacharyya, *Phys. Rev. Lett.* 96 (2006) 245503.
- [14] L.E. Tanner, R. Ray, C.F. Cline, *US Patent #3989517*.
- [15] L.E. Tanner, R. Ray, C.F. Cline, *US Patent #4050931*.
- [16] S.R. Elliott, *Physics of Amorphous Materials*, second ed., John Wiley & Sons Inc., New York, 1990, pp. 29-69.
- [17] G. Kumar, D. Nagahama, M. Ohnuma, T. Ohkubo, K. Hono, *Scripta Mater.* 54 (2006) 801.
- [18] A. Wiest, G. Duan, M.D. Demetriou, L.A. Wiest, A. Peck, G. Kaltenboeck, B. Wiest, W.L. Johnson, *Acta Mater.* 56 (2008) 2625.
- [19] G.J. Dienes, H.F. Klemm, *J. Appl. Phys.* 17 (1946) 458.
- [20] M.L. Lind, *Dissertation, California Institute of Technology* (2008).
- [21] E.C. Bingham, *Fluidity and Plasticity*, McGraw-Hill Book Company, Inc., Ohio, 1922, pp. 81-105.